

# Compact High-Redshift Galaxies Are the Cores of the Most Massive Present-Day Spheroids

Philip F. Hopkins<sup>1\*</sup>, Kevin Bundy<sup>1</sup>, Norman Murray<sup>2,3</sup>, Eliot Quataert<sup>1</sup>, Tod R. Lauer<sup>4</sup>, Chung-Pei Ma<sup>1</sup>

<sup>1</sup>*Department of Astronomy, University of California Berkeley, Berkeley, CA 94720*

<sup>2</sup>*Canadian Institute for Theoretical Astrophysics, 60 St. George Street, University of Toronto, ON M5S 3H8, Canada*

<sup>3</sup>*Canada Research Chair in Astrophysics*

<sup>4</sup>*National Optical Astronomy Observatory, Tucson, AZ 85726*

Submitted to MNRAS, March 3, 2009

## ABSTRACT

Observations suggest that the effective radii of high-redshift massive spheroids are as much as a factor  $\sim 6$  smaller than low-redshift galaxies of comparable mass. Given the apparent absence of low-redshift counterparts, this has often been interpreted as indicating that the high density, compact red galaxies must be “puffed up” by some mechanism. We compare the ensemble of high-redshift observations with large samples of well-observed low-redshift ellipticals. At the same physical radii, the stellar surface mass densities of low and high-redshift systems are comparable. Moreover, the abundance of high surface density material at low redshift is comparable to or larger than that observed at  $z > 1 - 2$ , consistent with the continuous buildup of spheroids over this time. The entire population of compact, high-redshift red galaxies may be the progenitors of the high-density cores of present-day ellipticals, with no need for a decrease in stellar density from  $z = 2$  to  $z = 0$ . The primary difference between low and high-redshift systems is thus the observed low-density material at large radii in low-redshift spheroids (rather than the high-density material in high-redshift spheroids). Such low-density material may either (1) assemble at  $z < 2$  or (2) be present, but not yet detected, at  $z > 2$ . Mock observations of low-redshift massive systems suggests that the amount of low-density material at high redshifts is indeed significantly less than that at  $z = 0$ . However, deeper observations will be important in constraining the exact amount (or lack thereof) and distribution of this material, and how it builds up with redshift. We show that, without deep observations, the full extent of such material even at low redshifts can be difficult to determine, in particular if the mass profile is not exactly a single Sérsic profile. We discuss the implications of our results for physical models of galaxy evolution.

**Key words:** galaxies: formation — galaxies: evolution — galaxies: active — galaxies: ellipticals — cosmology: theory

## 1 INTRODUCTION

Recent observations suggest that high-redshift spheroids may have significantly smaller effective radii than low-redshift analogues of the same mass (e.g. Daddi et al. 2005; Trujillo et al. 2006a, 2007; Zirm et al. 2007; Toft et al. 2007; van Dokkum et al. 2008; Franx et al. 2008; van der Wel et al. 2008; Cimatti et al. 2008; Buitrago et al. 2008). The apparent differences are dramatic: the inferred effective radii are as much as a factor  $\sim 6$  smaller at fixed stellar mass in the most massive galaxies at  $z = 2$ . Whatever process explains this apparent evolution must be particular to this class

of galaxies: disk galaxies are not similarly compact at high redshift (Ravindranath et al. 2004; Ferguson et al. 2004; Barden et al. 2005; Somerville et al. 2008). As such, these observations represent a strong constraint on models of galaxy and bulge formation.

Relative to the abundance of massive galaxies today, there are not a large number of compact systems at high redshift. However, even if just  $\sim 10\%$  survived intact to  $z = 0$ , this would greatly exceed the observed number density of such systems in the local Universe (Trujillo et al. 2009). In fact, at fixed stellar mass, ellipticals with older stellar populations appear to have the largest radii (Gallazzi et al. 2006; Bernardi et al. 2007; Graves et al. 2009; van der Wel et al. 2009).

The challenge for both observations and models is therefore

\* E-mail: phopkins@astro.berkeley.edu

to understand how these high-redshift systems could evolve to become “typical” spheroids today. Their masses, number densities, and clustering dictate that they are the progenitors of the most massive ellipticals and BCGs today (Quadri et al. 2007; Hopkins et al. 2007c). These systems have much larger  $R_e$  and thus have lower effective densities  $\Sigma_{\text{eff}} = M_*/(< R_e)/(\pi R_e^2)$ . However, this does not necessarily mean that the physical densities are lower than those of the high-redshift systems. One way to increase  $R_e$  would be to uniformly “puff up” the profiles, lowering the physical density everywhere. This would imply that the central densities of massive high-redshift ellipticals would need to decrease by two orders of magnitude from  $z = 2$  to  $z = 0$ . Alternatively,  $R_e$  can change by just as much by adding a relatively small amount of mass at low surface densities and large radii, without affecting the central density at all. In other words, an evolving effective density does not necessarily imply an evolving physical density at all radii.

Buildup of an “envelope” of low-density material is expected as massive early-forming galaxies undergo late-time (major and minor) gas-poor mergers with later-forming, less-dense ellipticals, disks, and dwarfs (Gallagher & Ostriker 1972; Ostriker & Tremaine 1975; Hausman & Ostriker 1978; Weil & Hernquist 1994, 1996; Naab et al. 2007). This is a relatively efficient channel for size-mass evolution, yielding factor of several size evolution with only a factor 1.5 – 2 increase in stellar mass (Hopkins et al. 2009d). But this less dense material added at large radii does not significantly affect the high-density core,<sup>1</sup> and so these models predict that the dense, high-redshift systems should survive to become the central regions of (some fraction of) today’s massive ellipticals.

If, on the other hand, high-redshift systems evolved primarily by equal-mass dry mergers between equivalently dense spheroids, then this will “inflate” the profiles relatively uniformly. In this extreme case, effective radii and stellar mass both approximately double in the merger; high-redshift systems would be uniformly more dense than their low-redshift descendants (see e.g. Hernquist et al. 1993; Boylan-Kolchin et al. 2006).

Distinguishing between these possibilities, as well as other dynamical, stellar evolution, or observational effects that could lead to apparent size-mass evolution clearly depends on understanding in detail differences in the surface density profiles of spheroids as a function of radius, at low and high redshift. In this paper, we quantitatively compare low and high-redshift observations to constrain these scenarios and inform how systems are evolving from  $z \gtrsim 2$  to  $z \sim 0$ .

In § 2 we directly compare the observed profiles of high and low-redshift massive spheroids, and show that, at the same physical radii, their stellar surface mass densities are comparable. The massive, high redshift systems appear no different than the “cores” of today’s massive ellipticals. In § 3 we determine the distribution of maximum/central densities, and show that this has not evolved significantly from  $z = 0$  to  $z > 2$ . In § 4 we calculate the mass function (and global mass density) of these high-density “cores” at both low and high redshift. This allows us to quantitatively compare the abundance of high-density material observed at both low and high redshifts. We show that there is as much or more high-density material in the cores of massive spheroids at  $z = 0$  as is observed to be in place at  $z = 1 - 2$ . The difference between low and

high-redshift systems, we conclude, lies in the lack of observed low surface-density envelopes around the high-redshift systems. In § 5 we show that, although such envelopes are weaker at high redshifts, some caveats should be born in mind with respect to the determination of the mass in low-density material in high-redshift spheroids. We summarize our results and discuss their consequences for physical models of spheroid evolution in § 6.

Throughout, we assume a WMAP5 cosmology ( $\Omega_M = 0.27$ ,  $\Omega_\Lambda = 0.73$ ,  $h = 0.705$ ; Komatsu et al. 2009), but the exact choice makes no significant difference.

## 2 SURFACE DENSITY PROFILES OF ELLIPTICALS AT HIGH AND LOW REDSHIFT

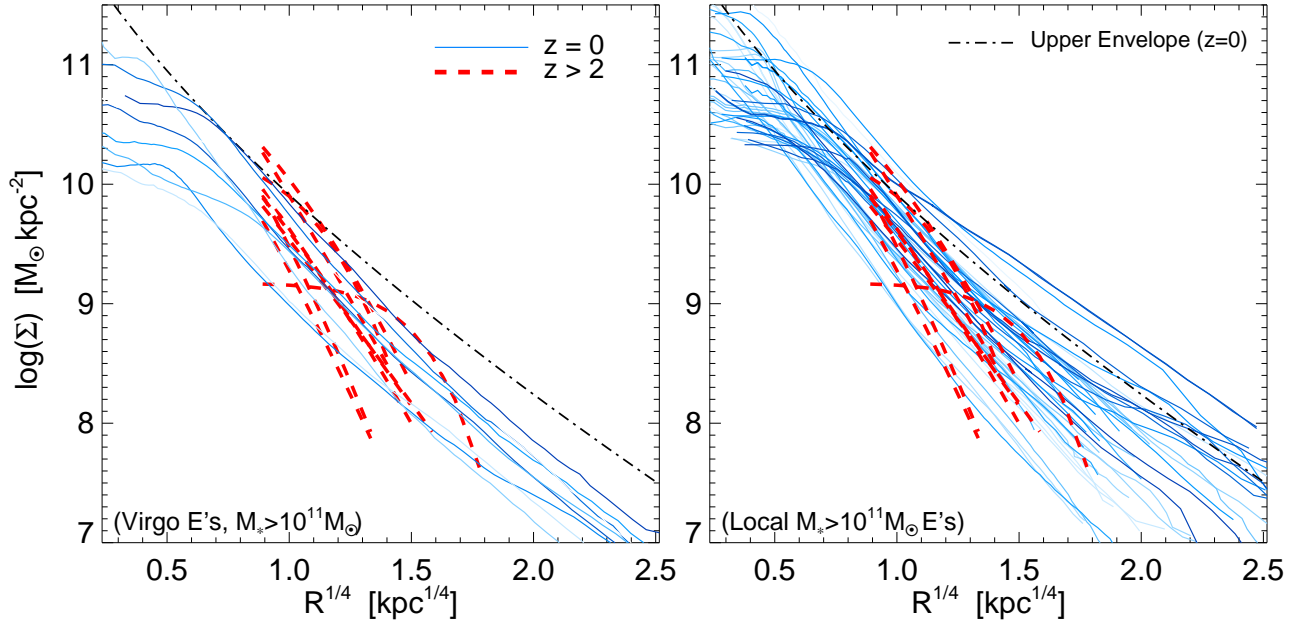
Figure 1 shows a direct comparison of the observed surface stellar density profiles of high-redshift compact galaxies and low-redshift massive galaxies. At low redshift we compile observed surface brightness profiles from Kormendy et al. (2009) and Lauer et al. (2007); this consists of a total of  $\sim 180$  unique local ellipticals with nuclear *HST* observations and ground-based data at large radii (allowing accurate surface brightness profile measurements from  $\sim 10$  pc to  $\sim 50$  kpc).<sup>2</sup> The isophotally averaged major axis profiles are measured in rest-frame optical; we convert to a stellar mass profile based on the measured total stellar masses and the assumption of a radius-independent stellar mass-to-light ratio. Conversion to stellar mass profiles using e.g. color or stellar population gradients and comparison of profiles from different instruments and wavebands in these samples are discussed extensively in Hopkins et al. (2009a, 2008a); the differences are much smaller than the scatter between individual profiles, and do not affect our conclusions. In Figure 1, we restrict our comparison to massive galaxies with  $M_* > 10^{11} M_\odot$ <sup>3</sup> because these systems are most likely to be descendants of massive high-redshift galaxies. The Kormendy et al. (2009) sample is a volume-limited survey of the Virgo spheroid population; as such it includes few very massive galaxies ( $M_* > 3 \times 10^{11} M_\odot$ ). The Lauer et al. (2007) galaxies are chosen to be representative of massive ellipticals in the local Universe, including more massive systems up to a couple  $10^{12} M_\odot$ . At the masses of interest, both are representative of the distribution of spheroid sizes in the local SDSS galaxy sample (Shen et al. 2003).

Figure 1 compares the low-redshift sample with the observed, PSF de-convolved profiles of nine high-redshift compact massive galaxies ( $M_* \gtrsim 10^{11} M_\odot$ ,  $R_e \sim 1$  kpc), specifically the  $z \sim 2 - 3$  sample from van Dokkum et al. (2008). This is a well-studied sample that represents the extreme of implied size evolution: the inferred average  $R_e$  is a factor of  $\sim 6$  smaller than local spheroids of the same mass. Figure 1 shows the best-fit Sersic profile of each galaxy in the sample; stellar mass-to-light ratios are determined by assuming a radius-independent  $M_*/L$  and normalizing the observed portion of the profile to the total stellar mass determined

<sup>1</sup> By “core,” we refer to the central regions of the galaxy, not to any specific class of central profile slopes. We use the phrases “cusp ellipticals” or “core ellipticals” to distinguish these.

<sup>2</sup> Note that although the composite (HST+ground-based) profiles were used in Lauer et al. (2007) to estimate effective radii, they were not actually shown in the paper.

<sup>3</sup> Stellar masses for all objects are determined from the combination of rest-frame optical and near-IR photometry, corrected to an assumed Chabrier (2003) IMF. We refer to Hopkins et al. (2009a) and Kriek et al. (2008b) for details of the low and high-redshift samples, respectively. Varying the specific bands used to determine stellar masses makes little difference, and changing the IMF will systematically change the stellar masses of all objects considered, but will not change our comparisons.



**Figure 1.** Direct comparison of the (major axis) surface stellar mass density profiles of  $z \geq 2$  compact massive spheroids ( $M_* \sim 10^{11} M_\odot$ , best-fit  $R_e \sim \text{kpc}$ ; red dashed) and local, massive ellipticals ( $M_* \geq 10^{11} M_\odot$ ,  $R_e \gtrsim 4 - 5 \text{ kpc}$ ; solid). Both  $\Sigma$  and  $R$  are in physical units. The high- $z$  profiles are the PSF de-convolved fit, plotted over the observed range in radius given the best-case limitations in seeing and surface brightness (from van Dokkum et al. 2008). The low- $z$  profiles combine space and ground-based photometry to obtain very large dynamic range; they are from the Kormendy et al. (2009) Virgo elliptical sample (*left*) and the Lauer et al. (2007) local massive elliptical sample (*right*). The former is a volume-limited sample, so contains fewer very massive galaxies with high central surface brightness. Although the high- $z$  systems have much smaller  $R_e$ , their densities at any physical radius are not unusual compared to the local objects: the central  $\sim 1 - 2 \text{ kpc}$  of massive ellipticals today are just as dense. The difference in  $R_e$  owes to the presence of the large wings/envelopes at low surface density in the low-redshift objects.

from photometry and spectroscopy in Kriek et al. (2006, 2008b,a). We plot the profile of each system over the maximum radial range observed: from the scale of a single pixel at the observed redshift to the limiting surface brightness depth of the best images. Both the low and high-redshift systems are plotted in terms of major-axis radii (a non-negligible correction).

At low redshift, the stellar mass-to-light ratios of ellipticals appear to be nearly independent of radius (reflected in e.g. their observed weak color gradients), but the stellar mass-to-light ratio may depend significantly on radius in the high-redshift systems (Trager et al. 2000; Côté et al. 2006; Sánchez-Blázquez et al. 2007). However, based on the observed stellar population gradients in local ellipticals, the observed ages/colors of the high-redshift systems, or the outcomes of numerical simulations, the expected variation in  $M_*/L$  is such that a young, recently-formed post-starburst stellar population at the center of the high-redshift galaxy will have higher  $L/M_*$  than older stars at larger  $R_e$  (see e.g. Hopkins et al. 2008b). This would make the high-redshift systems less dense than we assume here; we conservatively allow for the maximal stellar mass densities in those systems.

The comparison in Figure 1 is quite striking: although the best-fit effective radii and effective surface densities of the high-redshift systems are quite different from their low-redshift analogues, the actual stellar surface mass densities at any given observed radius do not appear significantly higher than a substantial fraction of the low-redshift population. In other words, inside the same observed radii  $\sim 1 - 5 \text{ kpc}$ , many of today’s massive ellipticals are just as dense as the high-redshift systems. The difference in effective radius stems primarily from the fact that the low-redshift systems have substantial extended wings/envelopes of low surface-

brightness material ( $\Sigma \ll 10^9 M_\odot \text{ kpc}^{-2}$ ); by contrast, the inference from fitting the high-redshift systems is that their profiles fall more rapidly at large radii (as we discuss further below).

For the sake of comparison with these and future high-redshift observations, it is useful to define the “upper envelope” of low-redshift galaxy density profiles. Formally, we can take e.g. the  $+1\sigma \approx 86\%$  contour of the combined sample of density profiles shown in Figure 1, but we find that this can be conveniently approximated with a simple Sersic function. This envelope is approximately given by

$$\Sigma_{+1\sigma}(z=0) \approx 4.5 \times 10^{12} M_\odot \text{ kpc}^{-2} e^{-11.67 \left( \frac{R}{40 \text{ kpc}} \right)^{1/6}}. \quad (1)$$

This is a Sersic profile with  $n_s = 6$ ,  $R_e = 40 \text{ kpc}$ , and total stellar mass  $M_* = 1.7 \times 10^{12} M_\odot$ . Note that most *single* galaxies do not remain along this envelope over its entire extent. Rather, at each radius, this represents the  $+1\sigma$  upper extent of observed densities within the spheroid population (i.e. the most dense systems at each radius); Most individual systems approach it over some more limited dynamic range. This is a useful comparison quantity in particular because, although the *mean* profiles of  $z = 0$  ellipticals are well-known, there has been relatively little parameterization of the scatter in profile shapes. Thus, even if high-redshift ellipticals are more dense than the median system today, if they do not exceed the relation given by Equation 1, then their densities can be accommodated within some portion of the present-day spheroid population, so long as they do not represent a large fraction of the present-day abundance of spheroids. As expected, we find that at their centers, the  $z = 2$  systems are at most comparable to this upper envelope, i.e. comparable to the most dense  $z = 0$  spheroid cores, and at large radii, they fall well below the envelope.

### 3 CENTRAL STELLAR DENSITIES

Figure 2 plots the *peak* surface stellar mass densities  $\Sigma_{\text{peak}}$  obtained in both the low and high-redshift galaxy populations. The “maximum” or peak surface density must be defined within some radius, for galaxies whose surface density continues to rise to unresolved radii (e.g. cusp ellipticals; although most of the local massive galaxies are core ellipticals, with relatively flat maximum surface densities within  $\sim 50 - 500$  pc). For example, the maximum stellar surface density can be defined as the average  $\Sigma$  interior to some fixed small radius  $\sim 50 - 100$  pc, or a fixed fraction of  $R_e$  from  $\sim 0.02 - 0.04$ , or by extrapolation to  $R = 0$  of a best-fit Sersic profile – we are simply interested in comparing the central densities at small radii in both low and high-redshift systems. For each determination, we find qualitatively similar results albeit with some small normalization differences; Figure 2 shows  $\Sigma_{\text{peak}}$  determined from averaging within 50 pc and within  $0.02 R_e$ . For the high-redshift systems, PSF and seeing effects smear out the maximum observed surface brightness/density inside  $\sim 1$  kpc; we extrapolate the best-fit Sersic profiles inwards to the same radii as the local systems. Making this same approximation in the low-redshift samples shows that it is reasonable, but tends to slightly over-estimate the central surface density, especially in core ellipticals.

At both low and high redshift, there is a characteristic maximum central surface stellar mass density  $\sim 0.3 - 2 \times 10^{11} M_{\odot} \text{ kpc}^{-2}$ , with significant, but still surprisingly little scatter given the known diversity in the profile shapes of ellipticals (e.g. variation in Sersic indices and cusp versus core populations). The maximum is similar whether we include ellipticals of all masses ( $\sim 10^9 - 10^{12} M_{\odot}$ ), or restrict to cusp or core populations; although dry mergers are expected to transform cusp ellipticals into core ellipticals via “scouring” (ejecting mass from the central regions in a BH-BH merger), this primarily affects the mass profile on very small scales (comparable to or less than the scales here – well below what we generally refer to as the “central” regions of ellipticals at  $\sim$  kpc scales). The maximum surface density of the high-redshift systems is perhaps a factor  $\sim 2$  larger than that of low-redshift systems, but given that we are extrapolating Sersic profiles inwards for the high-redshift systems, this is probably an upper limit. Thus while the observations imply up to a factor  $\sim 40$  evolution in effective surface brightness, there is nowhere near this much evolution in the true maximum stellar surface density, a much more physically relevant quantity.

Recently, Bezanson et al. (2009) reached very similar conclusions from a similar comparison between high and low-redshift profiles, using a different methodology and low-redshift sample. One subtle difference between our conclusions and theirs is that they claim the central densities of the high redshift systems appear higher, on average, than those at low redshifts by a small factor ( $\sim$  a couple). This owes largely to the fact that the authors extrapolate the best-fit Sersic profiles inwards to small radii – as we show here, this does lead to slightly higher central densities. But we caution that, doing the same in the low-redshift systems, we would obtain similar slightly higher densities: over the observed range (Figure 1) there is no difference. Moreover, Bezanson et al. (2009) compare the high-redshift profiles only with the average profile of similar-mass galaxies at low redshift; in Figure 1 and § 4 we consider the full distribution of profile shapes at low redshift: even if the high-redshift systems have, on average, slightly higher central densities, they are still compatible with the central densities of a large fraction of the  $z = 0$  massive elliptical population.

It is worth noting that the mass and redshift-independence in

$\Sigma_{\text{peak}}$  in Figure 2 is somewhat surprising, given the diversity of formation histories and scatter in e.g. the mass present at larger radii (see e.g. Hopkins et al. 2009e). A more detailed discussion of this will be the subject of future work, but it may relate to the maximum surface density of gas that can turn into stars (see § 6).

### 4 THE MASS AT HIGH STELLAR DENSITIES

We now quantify the amount of mass at different stellar surface densities. In order to reduce the effects of noise and PSF effects (important in particular for the high-redshift systems), we define the surface density in this section as the average surface density within each radius, i.e.  $\Sigma(R) = \langle \Sigma(< R) \rangle = M_*(< R)/\pi R^2$ . We obtain similar results using the local  $\Sigma$ , but with larger noise. For each observed system in our low-redshift sample, given the stellar mass profile (Figure 1), we calculate the total fraction of the stellar mass that lies above a given threshold in surface density  $\Sigma_{\text{min}}$ . We evaluate this for each system separately, and in Figure 3 we plot the average mass fraction at each  $\Sigma$  for all observed systems in our sample, in several bins of total stellar mass. Although the mass fraction above each  $\Sigma_{\text{min}}$  can vary by a large amount from galaxy to galaxy, the average is surprisingly robust across masses (and does not depend significantly on whether we include both cusp and core ellipticals or evaluate the two separately). By sufficiently low  $\Sigma_{\text{min}}$  thresholds,  $\sim 10^8 M_{\odot} \text{ kpc}^{-2}$ , essentially all mass in spheroids is accounted for; some systems have more extended, lower surface-brightness envelopes, but they contribute little total mass. Approximately  $\sim 25\%$  of the stellar mass density at each mass remains above  $\sim 10^{10} M_{\odot} \text{ kpc}^{-2}$  – a typical effective surface brightness for high-redshift ellipticals – in moderately high-mass systems (dropping to  $\sim 10\%$  by the most massive  $10^{13} M_{\odot}$  systems). By a threshold of  $\sim 10^{11} M_{\odot} \text{ kpc}^{-2}$ , we have reached the maximum/peak surface densities of ellipticals (Figure 2), and the mass fractions at higher densities drop rapidly.

The best-fit Sersic profiles of the  $z \sim 2$  systems imply that they have higher mass *fractions* above a high surface density threshold  $\sim 10^{10} M_{\odot} \text{ kpc}^{-2}$ . However, as illustrated above, this primarily owes to their having less mass at low  $\Sigma$ , not more at high  $\Sigma$ .

The comparison between the low and high-redshift samples can be made more quantitative by determining the stellar mass function above a given surface density threshold. To do so, we ignore all stellar mass in the Universe below a given threshold in  $\Sigma$ , and construct the spheroid mass function. The mass of a given galaxy is only the mass above that  $\Sigma$ ; i.e. we calculate the volumetric number density of spheroids with  $\Sigma > \Sigma_{\text{min}}$

$$n[> M_{\text{gal}}(> \Sigma_{\text{min}})] \equiv \frac{dN(\text{galaxies} | M_i > M_{\text{gal}})}{dV} \quad (2)$$

as a function of the integrated mass above  $\Sigma_{\text{min}}$ ,

$$M_i \equiv M(> \Sigma_{\text{min}}) = \int_{\Sigma=\Sigma_{\text{min}}}^{\Sigma \rightarrow \infty} \Sigma \times 2\pi r dr. \quad (3)$$

The resulting mass functions are shown in Figure 4. In detail, we take the observed stellar mass function of spheroids (Bell et al. 2003), and at each mass, convolve with the distribution of surface density profiles from Kormendy et al. (2009) and Lauer et al. (2007) for systems of the same mass, to determine the resulting mass function (number density) above a given surface density threshold.<sup>4</sup> We are assuming that the distribution of profile shapes

<sup>4</sup> Note that “density” here has two meanings: the volume density (the y-

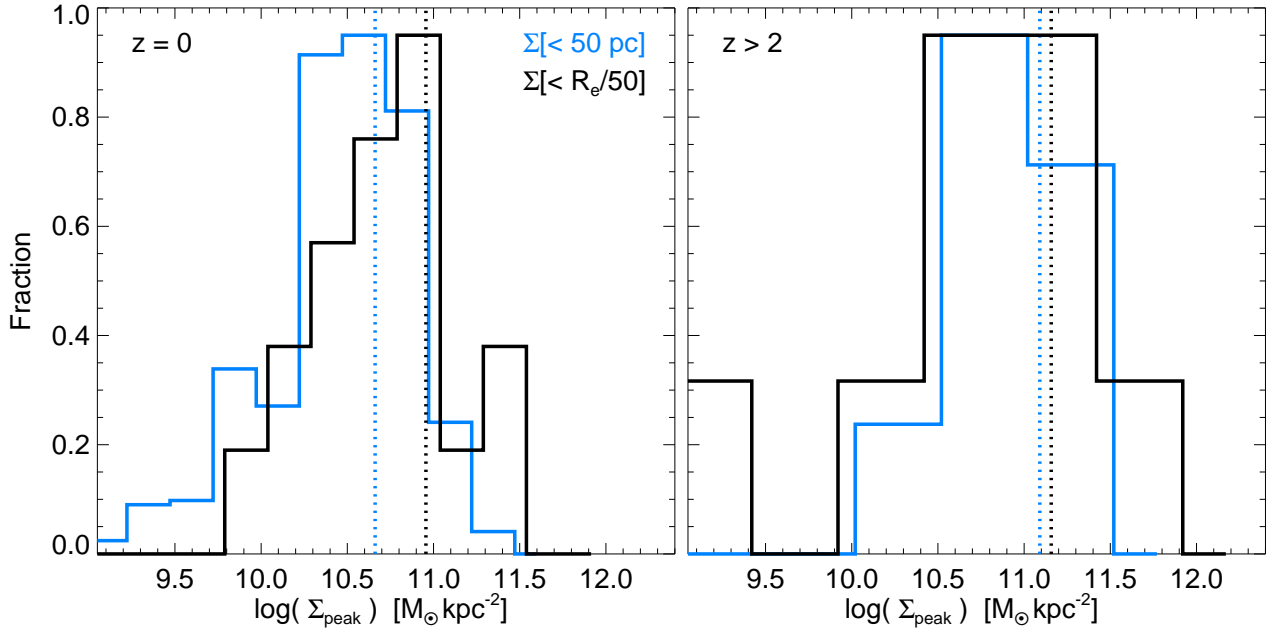


**Figure 2.** Distribution of peak (maximum) spheroid stellar mass surface densities. *Left:* Low- $z$  systems from Figure 1. Most ellipticals, at any mass, have  $\Sigma_{\text{peak}} \sim 0.3 - 1 \times 10^{11} M_{\odot} \text{ kpc}^{-2}$ . Histograms show two different calculations of  $\Sigma_{\text{peak}}$  (within 50 pc and  $R_e/50$ ); dotted lines are the median from each. *Right:* Same, for the high- $z$  samples. Direct observations are PSF and seeing-limited, so we extrapolate the best-fit Sersic profile inwards to obtain  $\Sigma_{\text{peak}}$  (this is typically an upper limit in the low- $z$  samples). The results are striking: central densities are reasonably independent of redshift.

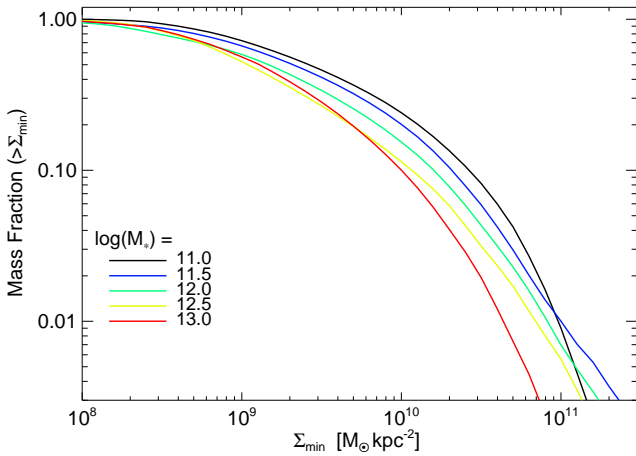


**Figure 3.** Average mass fraction above some threshold surface stellar mass density  $\Sigma_{\text{min}}$ , for the low- $z$  sample from Figure 1. The values shown are the average fraction of *all* spheroid mass (in a narrow range around each  $M_*$ ) above the given  $\Sigma_{\text{min}}$ . A significant fraction of the  $z = 0$  spheroid mass ( $\sim 25\%$ ) resides in matter at the inferred effective  $\Sigma$  of the high- $z$  compact systems ( $10^{10} M_{\odot} \text{ kpc}^{-2}$ ).

in Kormendy et al. (2009) and Lauer et al. (2007) are representative at each mass. Their sample selection as well as other measurements (see those works and e.g. Trujillo et al. 2002; Ferrarese et al. 2006; Allen et al. 2006) and the close agreement in fundamental plane correlations and Sersic index distributions in larger volumes (e.g. Shen et al. 2003) suggest that this is probably a good assumption.

axis of Figure 4) is the total number of galaxies meeting a given criteria per unit volume; the surface density is the local stellar surface mass density of stars within a particular galaxy.

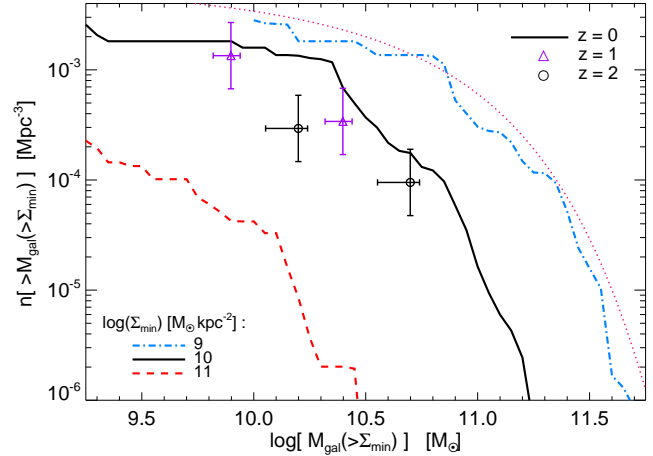


**Figure 4.** Spheroid stellar mass function (number density) for mass above a given surface stellar mass density threshold ( $\Sigma_{\text{min}}$ ). We calculate the  $z = 0$  mass function of spheroids including *only* stellar material in any galaxy above the given  $\Sigma_{\text{min}}$ , given the total stellar mass function and the observed distribution of profile shapes. The magenta dotted line shows the total spheroid mass function (Bell et al. 2003) – most of the mass is accounted for above  $10^9 M_{\odot} \text{ kpc}^{-2}$ . The value of  $\Sigma_{\text{min}} = 10^{10} M_{\odot} \text{ kpc}^{-2}$  corresponds to the effective surface density of the compact high-redshift spheroids; points show the results of the same calculation for the observed high-redshift systems and this value of  $\Sigma_{\text{min}}$ . We show this for the  $z \sim 2.3$  data from van Dokkum et al. (2008, black circles) and  $z \sim 1$  data from van der Wel et al. (2008, triangles).

Unsurprisingly, Figure 4 shows that at lower  $\Sigma$  thresholds the predicted mass function converges to the total stellar mass function of spheroids, i.e. most stellar mass is accounted for. And at high thresholds it drops rapidly, especially at high masses:  $10^{11} M_{\odot} \text{ kpc}^{-2}$  is the peak surface density inside  $\ll 1 \text{ kpc}$  at both

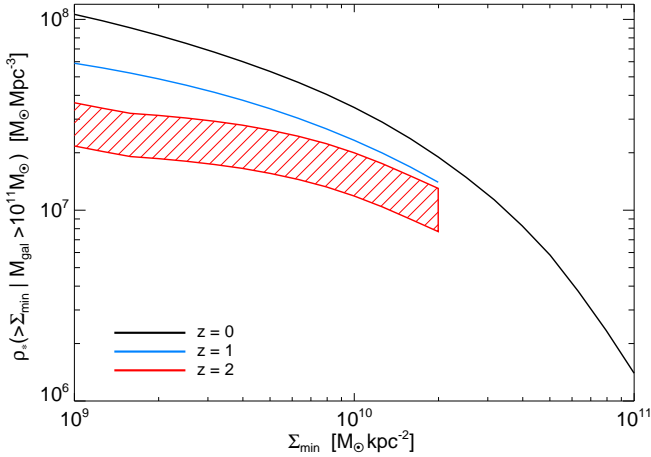


**Figure 5.** The total global mass density of stars which reside in massive galaxies (*total* galaxy mass  $> 10^{11} M_{\odot}$ ) and are above a threshold stellar mass surface density (within the galaxy) of  $\Sigma_{\min}$ . This is the integral of Figure 4, including only massive galaxies. We show the results from observations at  $z = 0$  (black),  $z = 1$  (blue) and  $z = 2$  (red; shaded range corresponds to typical uncertainties in the total mass density of these compact high- $z$  systems). The high- $z$  data is limited to the highest  $\Sigma$  directly observed (limited by resolution and seeing). At  $z = 0$ ,  $\sim 4 \times 10^7 M_{\odot} \text{Mpc}^{-3}$  is locked in massive ellipticals above a surface density of  $> 10^{10} M_{\odot} \text{kpc}^{-2}$ . This is a factor of a few larger than the mass density at such  $\Sigma$  at  $z \sim 2$ .

low and high redshifts – no observed systems have significant amounts of mass  $> 10^{11} M_{\odot}$  above this threshold.

In Figure 4 we compare the  $z = 0$  volume density of mass at  $\Sigma > 10^{10} M_{\odot} \text{kpc}^{-2}$  (solid lines) with observational inferences at  $z = 1$  (diamonds) and  $z = 2$  (circles). Specifically, given the *total* number density of  $> 10^{10} M_{\odot}$  spheroids/compact red systems at these redshifts (Pérez-González et al. 2008b), convolved with the distribution of profile shapes from van Dokkum et al. (2008), we obtain the number density of objects with mass above the relevant  $\Sigma$  threshold. In the error budget in Figure 4, we include the difference in number densities estimated by Fontana et al. (2006), van Dokkum et al. (2006), and Marcesini et al. (2008), and variation in the distribution of profile shapes/sizes fitted in other works, including Trujillo et al. (2007); Toft et al. (2007); Buitrago et al. (2008); Cimatti et al. (2008). These yield similar conclusions to within a factor  $\sim 2 - 3$ . At the masses of interest, the observations should be reasonably complete to these high surface densities.

We can also integrate the mass functions in Figure 4 to obtain the total volume density of stellar mass in spheroids above some threshold in surface density  $\Sigma_{\min}$ ; this is shown in Figure 5. Whereas mergers will not conserve number density, they should conserve total stellar mass in this calculation (to the extent that they do not change the  $\Sigma_{\min}$  of the central regions of galaxies). Since the high-redshift systems are primarily massive,  $> 10^{11} M_{\odot}$ , and their descendants cannot presumably be much lower mass, we restrict this calculation to only systems with a *total* stellar mass above this limit (although this only removes the very lowest-mass contributions to the high- $\Sigma$  population in Figure 4, and does not substantially affect our comparison). We then calculate, in systems above this mass, the total stellar mass above each threshold  $\Sigma_{\min}$ .

Figure 5 shows that there is  $\sim 4 \times 10^7 M_{\odot} \text{Mpc}^{-3}$  of stellar mass in  $> 10^{11} M_{\odot}$  ellipticals, above a surface density threshold of  $\Sigma > 10^{10} M_{\odot} \text{kpc}^{-2}$  in the local Universe. This is comparable to the *total* stellar mass density of high-redshift red spheroids (Labbé et al. 2005; van Dokkum et al. 2006; Grazian et al. 2007;

Abraham et al. 2007). Convolving over the observed size distribution at  $z \sim 2$ , the mass density above this threshold  $\Sigma$  is of course lower  $\sim 1 - 2 \times 10^7 M_{\odot} \text{Mpc}^{-3}$ . We obtain a similar result comparing to the  $z = 1$  observations from van der Wel et al. (2008), with the relevant constraints being at lower surface density as there is less relative evolution.

Our comparisons indicate that the local Universe contains just as much, or more, stellar mass at high surface densities as implied by observations of high-redshift systems. It is thus possible that all of the high-stellar mass density systems at high redshift can be incorporated into massive ellipticals today, without any conflict with their observed number densities or surface brightness profiles. In fact, a reasonable amount of high-surface density material must continue to be added to the elliptical population, perhaps by gas-rich mergers, from high redshifts until  $z = 0$ . It is the subject of another study whether gas-rich mergers produce an adequate amount of high- $\Sigma$  stellar mass in current galaxy formation models to account for the observed growth of  $\rho_*$  in Figure 5. Nonetheless, the high density material at high redshifts is not inconsistent with the  $z \sim 0$  data and therefore does not have to “go away.”

## 5 THE MASS AT LOW STELLAR DENSITIES

Our results demonstrate that the difference between low and high-redshift spheroids does not arise in their central densities, but in the large envelopes of low surface brightness material observed in low-redshift systems. This is the origin of their larger effective radii.

There are two natural ways of reconciling the low and high-redshift observations with the hypothesis that the high-redshift spheroids are the progenitors of today’s ellipticals. First, the high-redshift systems may not have much low-density material at large radii; low-density material would then have to be accreted at lower redshifts via late-time mergers (minor or major) with gas-poor disks and ellipticals (i.e. lower-density systems). Such a scenario is feasible, and indeed expected – if the initial spheroid-forming mergers are sufficiently gas-rich, there will be little low-density material from extended stellar disks to contribute to an extended envelope (Hopkins et al. 2009a). And comparison of clustering properties, merger rates, and stellar populations all imply that these massive, high redshift systems *should* grow by a factor  $\sim 1.5 - 2$  via these channels between  $z \sim 2$  and  $z = 0$ , more or less sufficient to account for the envelopes seen in Figure 1 (see e.g. van Dokkum 2005; Bell et al. 2006; Zheng et al. 2007; Lin et al. 2008; Conroy & Wechsler 2009).

The second way of reconciling the low and high-redshift observations is that high-redshift systems do have material at low surface densities already, but it is not seen in present observations (in such a case, there would be much less than expected of a buildup of low-density material). In order to be as conservative as possible, in considering the possible degree of envelope buildup since high redshifts, we consider this possibility here.

Figure 6 illustrates circumstances under which the high-redshift observations may not be sensitive to extended, low- $\Sigma$  wings. We consider a few representative galaxy profiles from the local sample of Kormendy et al. (2009), ranging from low-mass cusp ellipticals with low Sérsic indices at large radii (steep surface density falloff), to high-mass core ellipticals with high Sérsic indices at large radii (extended envelopes).<sup>5</sup> For each, we convolve

<sup>5</sup> The specific five galaxies shown are (from top to bottom) NGC 4464,



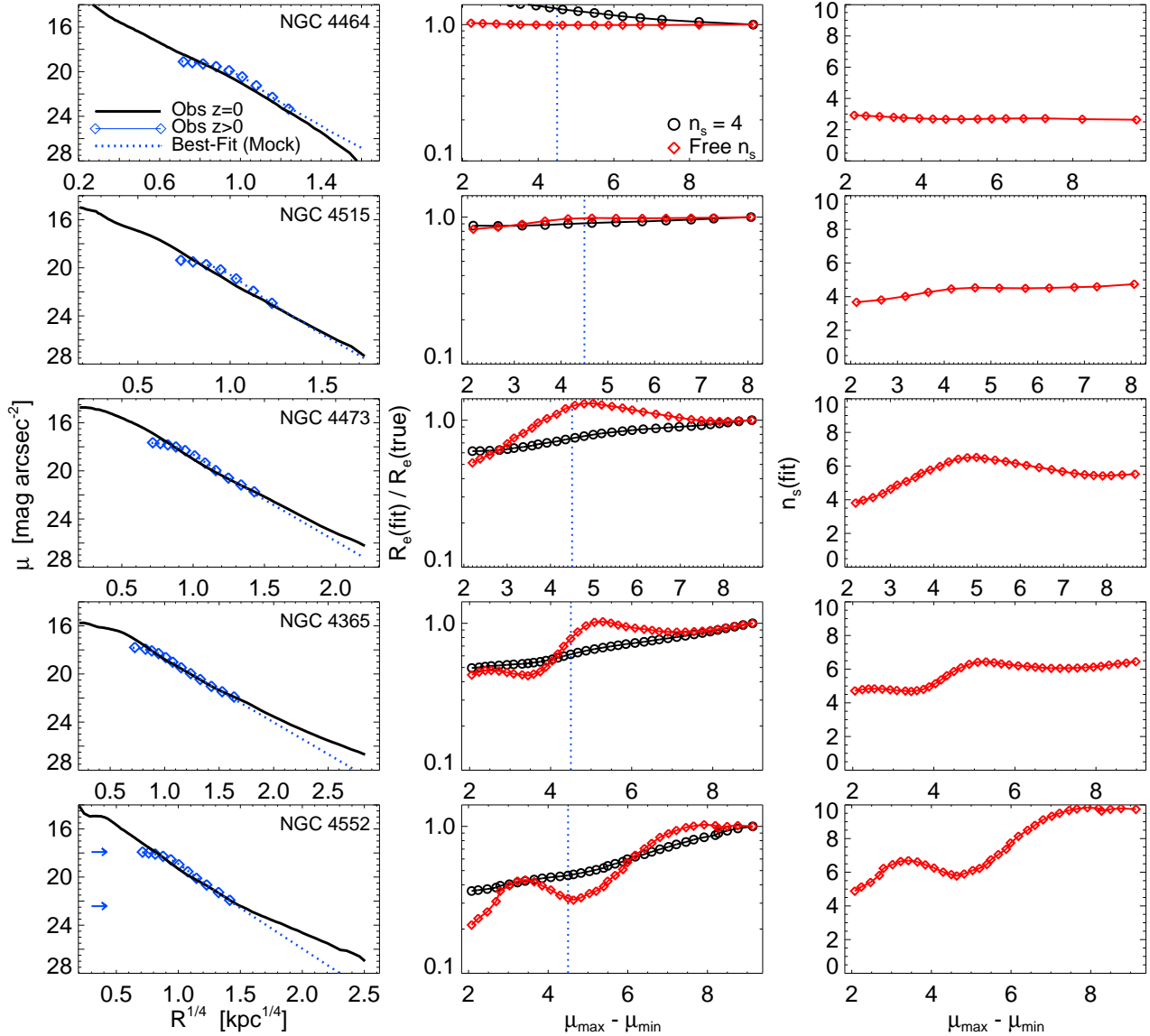


**Figure 6.** Best-fit light profile parameters  $R_e$  and  $n_s$  versus image depth. *Left:* Observed (V-band) surface brightness profiles (black) for several typical local spheroids in the Kormendy et al. (2009) sample,<sup>5</sup> from low mass (low- $n_s$ , i.e. steep light profile decay; *top*) to high mass (high- $n_s$ , i.e. shallow decay/large envelope; *bottom*). These are compared to the profiles constructed from mock images of the same objects with best-case imaging available at  $z \sim 0.5 - 2$  (cyan diamonds; seeing/PSF FWHM of 1.2 kpc, and depth/dynamic range of  $\mu_{\max} - \mu_{\min} = 4.5$  mag; arrows in *bottom left*). Dotted cyan line shows the best-fit (convolved) Sersic profile fit to the mock high- $z$  imaging data, extrapolated to large radii. *Center:* Effective radii of the best-fit Sersic profile, relative to the true  $R_e$ , as a function of image depth. We construct a series of mock profiles with similar PSF, seeing, noise, and pixel size (as *left*), but vary the image depth  $\Delta\mu \equiv \mu_{\max} - \mu_{\min}$ . We fit the resulting mock profile (with each  $\Delta\mu$ ) with either a free Sersic index  $n_s$  (red diamonds) or fixed  $n_s = 4$  (black circles). Dotted vertical line shows the  $\Delta\mu$  of the mock profile at *left*. *Right:* Corresponding best-fit  $n_s$  (for free- $n_s$  fits). At low masses (little stellar envelope), there is little dependence on the image depth. At high masses (large-envelope systems) a strong trend appears, because the  $z = 0$  profiles of massive galaxies are fundamentally *not* well-described over a large dynamic range by single Sersic laws. At small  $R \lesssim 2 - 10$  kpc ( $\Delta\mu \sim 2 - 4$ ), the radii that dominate the fit in all but the deepest local imaging data, the profiles show a steeper falloff (indicative of  $n_s \lesssim 4$ , weak-envelope profiles) and yield a smaller best-fit  $R_e$ . Only at  $R \gtrsim 20 - 50$  kpc ( $\Delta\mu \sim 6 - 8$ ) do the low-density wings appear, leading to larger  $n_s$  and  $R_e$ .

NGC 4515, NGC 4473, NGC 4365, and NGC 4552. The first three are classified as cusp ellipticals, the latter two as core ellipticals. The observations are described in Kormendy et al. (2009), but typically include  $\sim 80 - 100$  photometric points from a few pc to  $\sim 50$  kpc in radii; photometric errors are  $\lesssim 0.04$  mag arcsec $^{-2}$  (not visible in Figure 6). They have stellar masses of  $M_* = (0.17, 0.13, 1.2, 3.9, 2.0) \times 10^{11} M_\odot$ , true effective radii – fit from the full data with proper multi-component profiles – of  $R_e = (0.60, 1.05, 3.19, 14.6, 10.6)$  kpc, and central velocity dispersions of  $\sigma = (120, 90, 192, 271, 252)$  km s $^{-1}$ . Fitting their *outer* profile shapes to

the observed profile with a simple Gaussian PSF with typical best-case resolution for the high-redshift observations of interest ( $1\sigma = 0.5$  kpc; FWHM 1.2 kpc). We then fit the (one dimensional) profile to a *single* Sersic profile (fitting appropriately convolved model profiles). We do this as a function of image depth. Specifically we

Sersic profiles (where they are uncontaminated by the central, high surface-density components; see e.g. Hopkins et al. 2009a,d) yields best-fit outer Sersic indices of  $n_s = (2.1, 3.9, 4.6, 7.1, 9.2)$ .

plot the results of the fits as a function of  $\Delta\mu \equiv \mu_{\max} - \mu_{\min}$ , the surface brightness ( $\text{mag arcsec}^{-2}$ ) of the deepest point included relative to the central/maximum surface brightness of the convolved image. In Figure 6 we plot the resulting best-fit effective radii, considering both fits with a free Sersic index  $n_s$  and a fixed  $n_s = 4$ . For fits with a free  $n_s$ , we plot the corresponding best-fit  $n_s$ .

For low-mass and intermediate-mass galaxies, which have low  $n_s$  and therefore fall off steeply in  $\Sigma$  at large  $R$ , the true profiles can be recovered with even relatively shallow observations. If anything, for the lowest mass-galaxies, which have Sersic profile indices  $n_s \sim 2 - 3$  (when fit in this manner to a single Sersic index; see e.g. Balcells et al. 2007b,a; Ferrarese et al. 2006), the effects of the PSF tend to slightly *increase* the inferred effective radius in shallow images. For systems very close to  $n_s = 4$ , characteristic of intermediate-mass galaxies, there is almost no depth-dependent bias to the inferred  $R_e$  and  $n_s$  (see NGC 4515 in Figure 6). The same conclusions are reached in the analysis of mock-redshifted SDSS images of low-mass galaxies in van der Wel et al. (2008). In short, if there is not a pronounced low-surface brightness envelope, then whether or not the low-surface brightness data is well-observed makes little difference to the fitted properties. Again, we emphasize, for *normal*  $\sim L_*$  ellipticals, there appears to be no bias, and the relevant parameters are recovered well via simple Sersic fits, even given a very limited dynamic range of fitting.

However, in the most extreme systems characteristic of the most massive galaxies – those with large outer Sersic indices indicative of extended envelopes that include significant low-density material out to  $\sim 100$  kpc radii – the inferred  $R_e$  and  $n_s$  can be sensitive to whether or not this material is included in the fits. Considering the entire sample, we find that the typical depth required to obtain a “converged”  $R_e$  and  $n_s$  (to within  $\sim 30 - 50\%$  of the value obtained with the deepest available data) is a strong function of stellar mass (really, the strength of the low-density envelope), rising from  $\Delta\mu \sim 4$  mag in intermediate-mass systems to  $\Delta\mu \sim 6 - 8$  in high-mass ( $M_* > 10^{11} M_\odot$ ) systems. If we require that at least 50% of local systems have converged  $R_e$ , we obtain the approximate mass-dependent criteria  $\Delta\mu_{\text{conv}} > 3.0 + 2.3 \log(M_*/10^{11} M_\odot)$ ; if we raise our desired threshold to  $\sim 75 - 90\%$ , the minimum  $\Delta\mu$  should be uniformly deeper by another 1.5 mag. In terms of physical radii, depth of  $\Delta\mu \sim 4$  mag corresponds roughly to a maximum well-sampled, high  $S/N$  physical radius of  $\sim 5$  kpc; the depth required for obtaining converged  $R_e$  in massive systems ( $6 - 8$  mag) corresponds to physical radii  $\gtrsim 20 - 50$  kpc.

This bias arises because the systems with large envelopes are *not* perfect Sersic profiles; indeed, it is now well-established that *no* populations of spheroids are completely described by single Sersic profiles given sufficient dynamic range (see e.g. Kormendy 1999; Ferrarese et al. 2006; Lauer et al. 2007; Côté et al. 2007; Kormendy et al. 2009). As a consequence, although a single Sersic profile is often a formally good fit (in a  $\chi^2$  sense) over limited dynamic range, the best-fit  $n_s$  can change systematically as that dynamic range changes. The effect is most pronounced in systems with the most dramatic envelopes; at small radii  $R \lesssim 2 - 10$  kpc, systems are either “concave down” (which corresponds to a local Sersic index  $n_s < 4$ ) or uncurved ( $n_s = 4$ ). At larger radii, the profiles become more “concave up” ( $n_s > 4$ ). It is important to stress that, as such, the “correct” Sersic index is fit for the dynamic range sampled in the simple examples shown. If, in fact, the high-mass systems shown in Figure 6 were perfect Sersic profiles, there would be no significant effect. Ultimately, this reflects the obvious caveat to any limited dynamic-range observation: a fit is being extrapo-

lated to radii not directly observed, based on some assumed functional form.

We emphasize that Figure 6 is intended to be purely illustrative; we are *not* attempting to construct a specific comparison with or calibration for any individual observed sample. The specific calibrations for these observations are different sample to sample, and well outside the scope of this paper – we refer to the relevant observational papers for more details. For example, the real fit results will also depend on the resolution, instrument PSF, sky subtraction, and other details. Given the non-trivial dependence of profile shape curvature on radius in the most extreme systems, the results will depend just as much on the relative weighting (error bars as a function of radius) in the observed profile as on any choice of a “cutoff” radius (recall, we simply truncate the profile at some limit – realistically, this will appear as some surface-brightness-dependent error bar). Moreover, in many works (e.g. Trujillo et al. 2007; van Dokkum et al. 2008; Buitrago et al. 2008), the best-fit Sersic profile is determined directly from a fit to the two-dimensional image data, assuming a (radius-independent) ellipticity. In other works (e.g. Kormendy et al. 2009; Lauer et al. 2007), the image data is used to produce a major-axis or circularized profile (which allows for e.g. variations in ellipticity with radius or isophotal twists) and then fit to a Sersic profile. The attendant systematics, at this level of detail, are not identical; and re-fitting the objects shown in Figure 6 in two-dimensional images tends to suppress the run of Sersic index with fitted radius (owing to the difference in relative error weighting; C. Peng, private communication). The consequences of those details can, in principle, affect the inferred sizes in either direction, not just towards inferring smaller sizes in lower-depth observations.

That being said, we can consider these caveats in the context of the deepest available observations at  $z \sim 1 - 2$ , spanning  $\Delta\mu \sim 3 - 4$  mag ( $S/N$  rapidly decreasing at  $R \gg 5$  kpc; see Trujillo et al. 2004; Cimatti et al. 2008; Damjanov et al. 2009). At these depths, our comparisons suggest that – if the “true” profiles were identical to those of today’s most extreme massive galaxies (again, systems with  $\sim 100$  kpc envelopes and very large  $n_s \sim 8 - 10$  – the effective radii could be under-estimated by factors up to  $\sim 2 - 3$ . It is not, in principle, hard to recover fitted  $R_e \sim 2 - 3$  kpc for such systems in this simplified experiment, for individual objects given limited dynamic range. Note, however, that the details are sensitive to the issues above: there is less of a discrepancy (in at least this idealized case), for example, comparing the two-dimensional profiles. More importantly, even allowing for this level of an effect, it is very difficult to account for the entire evolution observed; in short, there is a real deficit of low density material at large radii in the high-redshift systems. This is already apparent at the lowest  $\Sigma$  sampled, in e.g. Figure 1, where the high-redshift profiles are falling more rapidly than those of low-redshift analogues.

Again, if there is no large envelope as in the extreme case considered here, then there will be no bias in  $R_e$  in high-redshift observations. But of course, this becomes circular – the point is simply that caution is warranted extrapolating any profile (especially profile shapes calibrated to the observations of low-redshift galaxies) to radii not directly observed.

Other, simple tests can constrain these possibilities. For example, Zirm et al. (2007) stack  $\sim 14$  high-redshift ( $z \gtrsim 2$ ) systems identified as compact (gaining roughly an additional  $\Delta\mu \sim 1.5$ ), and see no significant change in Sersic profile or size (relative to the luminosity-weighted average size of the individual fits). Likewise, stacking the  $z = 1$  compact systems in van der Wel et al. (2008), the best-fit Sersic index is  $n_s \approx 4$ , comparable to the individual



fit results. These appear to support what can already be seen in Figure 1 (and Figure 1 of Bezanson et al. 2009); at the maximum radii  $\sim 5$  kpc sampled in the high-redshift observations, the profiles do appear to be falling more rapidly with radius than profiles of similar-mass low-redshift galaxies.

It appears, therefore, despite the caveats above, that there is a real deficit of material at low surface densities at large radii around massive, high-redshift galaxies.

However, it is important emphasize two simple points this highlights with respect to the interpretation of observed surface density profiles. First, some caution is always warranted when the dynamic range is limited. Additional checks, such as stacking the observed images, calibrating against low-redshift samples, and testing for bias in surface brightness limits of the sample, are important (and indeed have been a critical component of many of the high-redshift studies considered here). Given the lack of strong constraints on the amount of material at very low surface densities at high redshifts, the effective radii of the most extreme systems could (again, depending on the circumstances as noted above) be biased at the factor  $\sim 2$  level. This is insufficient to explain the total observed evolution – there appears to clearly be some real evolution in the amount of low surface density material – but it points to the still relatively large uncertainties in just “how much” low density material is (or is not) already in place at  $z = 2$ . Constraints on this quantity, in particular as a function of redshift, will be of considerable interest for constraining models of how low-density envelopes build up from high redshifts to today.

Second, it should be borne in mind that real ellipticals are not always perfect Sérsic profiles, and in some cases the best-fit profile shape can change depending on the dynamic range sampled. As such, direct comparison of profiles, such as that considered here or in e.g. Bezanson et al. (2009) are important (as opposed to just comparison of fitted quantities such as Sérsic index and effective radius). Moreover, inferences made from extrapolation of Sérsic fits should always be treated with some caution: the approach appears to work reasonably well with normal,  $\sim L_*$  galaxies, for inferring simple quantities such as the effective radius, but it ultimately depends on the *assumption* that the functional form of the Sérsic profile is a good description of the “true” profile at radii where the direct observational constraints are not as strong. For example, the approach of many works attempting to infer whether or not significant bias is present, by mock imaging systems modeled as single Sérsic profiles (artificially redshifting and imaging them, then re-fitting to a Sérsic profile), is a useful exercise, but does not necessarily capture all of the physical possibilities. Even at low redshifts, in fact, only a small fraction of massive ellipticals have effective radii that can be *directly* determined from the observations (i.e. converged  $R_e$  from the actual observed light profile, independent of fitting or extrapolation, that do not change as deeper radii are sampled; see e.g. the discussion in Kormendy et al. 2009). Extending these samples, in particular at low and intermediate redshifts, is important both for studying the low-density envelopes that build up at later times and for informing our interpretation of the high-redshift observations.

## 6 DISCUSSION

### 6.1 Can Yesterday’s Compact Spheroids Be the Cores of Today’s Ellipticals?

We have compared the stellar mass profiles of high-redshift, “compact” massive spheroids and well-studied local massive ellipticals.

There has been considerable debate in the literature regarding the origins and fate of the compact high-redshift systems: they appear to be smaller ( $R_e \sim 1$  kpc at  $\sim 10^{11} M_\odot$ ) than all but a tiny fraction of local, similarly massive galaxies which have  $R_e \sim 4 - 5$  kpc at  $z = 0$ . However, comparing the surface stellar mass density profiles directly, over the ranges that are actually well-sampled by observations, we show that the observed high-redshift systems have surface density profiles similar to the inner, dense regions of local massive ellipticals (Figure 1).

In other words, although the *effective* stellar mass surface density within  $R_e$ ,  $\Sigma_{\text{eff}} \equiv 1/2 M_*/(\pi R_e^2)$ , is large in high-redshift systems, the physical stellar surface densities are comparable to the typical central surface densities observed at radii  $\sim 0.5 - 5$  kpc in many local ellipticals. The centers or cores of local spheroids are just as dense as those of high-redshift systems: the difference is in the effective radii and effective densities, owing to the large, extended wings/envelopes of low surface brightness material around local massive spheroids. This material leads to a larger  $R_e$  and lower effective surface density in the local systems.

We have further shown that the distributions of the *maximum* stellar surface densities are nearly the same at  $z \sim 2$  and  $z = 0$  (Figure 2) – at small radii today’s ellipticals have similar maximum nuclear stellar surface densities of  $\sim 0.3 - 1 \times 10^{11} M_\odot \text{ kpc}^{-2}$  over a wide range in stellar mass from  $\sim 10^9 M_\odot$  to  $\gtrsim 10^{12} M_\odot$ . The high redshift systems have their central surface densities smeared out by PSF and seeing effects, and thus do not reach these densities at any observed point; but extrapolating their best-fit Sérsic profiles inwards they exhibit similar peak surface densities. Similar conclusions are reached by Bezanson et al. (2009) as well (note that the factor  $\sim$  a couple apparently higher densities those authors note in the central regions of high-redshift systems depends on extrapolating Sérsic profiles to smaller radii than observed, as well as ignoring the scatter in the central densities of ellipticals today). High-redshift red galaxies are thus not uniformly more dense; indeed, the maximum/peak surface density of spheroids does not appear to evolve significantly from  $z \gtrsim 2$  to  $z \sim 0$ .

Using a large sample of local, high-dynamic range observations, we have constructed a census of the local spheroid population and have quantitatively calculated the number of systems with central/core mass densities above a given surface mass density and stellar mass threshold (Figures 3-5). We have used this to construct the stellar mass function of spheroid “cores” – i.e. the stellar mass function of the parts of today’s ellipticals that lie above a given surface stellar mass density threshold.

The regime of particular interest is  $\Sigma \sim 10^{10} M_\odot \text{ kpc}^{-2}$ , which corresponds to the effective surface brightness of the high-redshift compact systems ( $10^{11} M_\odot$  with  $R_e = 1$  kpc). We find that  $\sim 25 - 35\%$  of the stellar mass density in  $z = 0$  massive spheroids lies above this surface density. Typical ellipticals have cores containing  $\sim 1 - 5 \times 10^{10} M_\odot$  above this threshold. Comparing this to the observed properties of massive galaxies at  $z = 1$  and  $z = 2$ , we find that by both number and total stellar mass, all of the high-redshift, compact systems can be accounted for in the cores of today’s ellipticals. For example, even in the extreme case in which every  $z = 2$ ,  $10^{11} M_\odot$  or larger spheroid (space density  $\approx 10^{-4} \text{ Mpc}^{-3}$ ) had  $R_e = 1$  kpc, this would correspond to the same space density of systems with  $> 1/2 M_* = 5 \times 10^{10} M_\odot$  above the effective surface density  $10^{10} M_\odot \text{ kpc}^{-2}$ . At  $z = 0$ , the space density of such massive, high surface density cores is a factor  $\sim 1.5 - 2$  higher. Doing the calculation more properly (convolving over the mass function and distribution of profile shapes), there is a factor  $\sim 2$  more mass in local massive cores than is present at  $z > 2$ ; the difference is

qualitatively similar, but smaller, comparing to  $z = 1$  populations. Not only can the high-redshift systems be accommodated (rather than being destroyed), but high density material in the centers of ellipticals may continue to build up even at relatively low redshifts.

## 6.2 How Does this Relate to Physical Models?

These conclusions are of considerable importance for physical models of spheroid formation and evolution, and in particular for the models that have been proposed to explain both the formation of high-redshift, apparently compact galaxies and their evolution into local  $z = 0$  systems.

Models for spheroid formation naturally predict that ellipticals and bulges are fundamentally two-component objects, with a dense, central core built by dissipational processes – the loss of angular momentum in a progenitor gas disk, which then falls to the center and turns into stars in a compact starburst – and an extended, lower-density envelope build by dissipationless processes – the violent relaxation of progenitor disk stars, observed to be at much lower phase-space densities than the compact cores of ellipticals (Mihos & Hernquist 1994; Hopkins et al. 2008a). Observations in the local Universe have confirmed much of this picture and made it increasingly robust (Kormendy 1999; Hibbard & Yun 1999; Rothberg & Joseph 2004; Kormendy et al. 2009). Indeed, simulations by several independent groups consistently find that it is not possible to make realistic ellipticals without the appropriate mix of these two components (Barnes & Hernquist 1996; Naab et al. 2006; Cox et al. 2006; Oñorbe et al. 2006; Jesseit et al. 2007; Burkert et al. 2008). As such, the existence of dense cores in spheroids at both low and high redshifts is a natural consequence of dissipational spheroid formation.

It is possible, if mergers are sufficiently gas-rich<sup>6</sup>, to build just the high-density core, and to add the envelope in relatively gas-poor mergers at later times. Given the gas-richness of high-redshift galaxies, some size evolution is naturally predicted in models, with high-redshift systems being more dominated by the dense, dissipational remnant (Khochfar & Silk 2006; Hopkins et al. 2009c).

The high-redshift observations represent an ideal opportunity to catch such cores “in formation” and strongly constrain their physical origin. Today, such cores are typically extremely old:  $\sim 10$  Gyr. At high redshifts, however, they have ages  $\lesssim 500$  Myr (Kriek et al. 2006). Understanding their stellar populations, metallicities, kinematics, and densities is critical to inform models of how dissipation builds the central regions of galaxies. There appears to be a natural link between the observed compact red galaxies and bright sub-millimeter galaxies, which are intense starbursts with consistent number densities (accounting for their short duty cycles) and physical sizes (Tacconi et al. 2006; Younger et al. 2007, 2008; Cimatti et al. 2008). This class of SMGs is widely believed to be the product of major mergers (Shapiro et al. 2008; Tacconi et al. 2008). Establishing further connections between these populations would not only enable new tests of the merger hypothesis, but would also rule out alternative models (e.g. monolithic collapse) for spheroid core formation.

The maximal mass densities of spheroids at both low and high redshift ( $\sim 10^{11} M_{\odot} \text{ kpc}^{-2}$ ), for example, may inform models of

star formation and feedback in extreme environments. This maximum surface density is intriguingly similar to previous suggestions of maximal (Eddington-limited) starbursts: if the observed mass surface density is initially pure gas, forming stars according to the Kennicutt (1998) relation (giving  $\sim 2500 M_{\odot} \text{ yr}^{-1} \text{ kpc}^{-2}$ ), this implies a luminosity  $= 1.5 \times 10^{13} L_{\odot} \text{ kpc}^{-2}$ . This is the Eddington limit for dusty systems (Thompson et al. 2005). And, interestingly, it corresponds to the maximum SFR surface density in dense SMGs (Tacconi et al. 2006; Younger et al. 2008). The fact that so few ellipticals scatter above this peak surface density also suggests that their centers may have formed in a few dissipational events – if Eddington-limited arguments explain these peak densities, then there is no reason why they could not be exceeded if the gas “trickled in” at a lower rate or in several smaller events. Clearly, it is of interest to investigate constraints on star formation and feedback models stemming from this.

Understanding the evolution in profile shapes, in particular how central versus outer densities evolve, is necessary to constrain how the potential and binding energy at the centers of spheroids evolve. This may be intimately related to the BH-host galaxy correlations in feedback-regulated models of BH growth (see e.g. Hopkins et al. 2007b,a, and references therein). There has been considerable debate regarding the state of the BH-host correlations at these redshifts: better understanding of spheroid cores that dictate the local potential depth is critical to inform theoretical models.

Current observations suggest that a large fraction of the high-density material in spheroids was assembled at early times. Although we have shown that it is possible to accommodate the mass in dense, high redshift cores in the elliptical population today, the observations suggest that of order half the massive cores of today’s massive ellipticals had to be in place by  $z > 2$ . Compare this to just  $\sim 5\%$  of the total spheroid mass density in place at these redshifts, and  $\sim 20\%$  of the massive galaxy ( $> 10^{11} M_{\odot}$ ) density (Grazian et al. 2007; Pérez-González et al. 2008b; Marchesini et al. 2008). In other words, it appears that the massive cores of today’s ellipticals assembled preferentially early. This is qualitatively consistent with models of dissipational formation, but in semi-analytic models explaining early massive elliptical formation is quantitatively quite challenging (see e.g. Bower et al. 2006; Fontana et al. 2006). The observations thus constrain not just the total assembly, but how this takes place – invoking early minor mergers or gas-poor processes, for example, might be able to account for the shape of the mass function, but would not explain the early formation of dense cores.

The observational comparison here favors models in which high-redshift compact galaxies are not destroyed (as has typically been concluded), but accrete or reveal previously “hidden” extended envelopes of low surface-brightness material. Their central densities remain, but with the appearance of low-density material, the effective radii and profile shapes quickly become comparable to massive galaxies today. If the high redshift systems genuinely do not have such low-density envelopes, the required evolution is only a factor  $\sim 1.5 - 2$  growth in stellar mass from high redshifts to today. Indeed, dry mergers onto such massive, early-forming systems are cosmologically inevitable, and the mass growth requirements found here are consistent with the current stellar mass function constraints (Brown et al. 2008; Pérez-González et al. 2008a). Moreover most dry mergers in such massive systems will be with later-forming, less massive and less dense systems, that are not expected to disrupt the dense cores, but will instead build up an envelope of lower surface density material (see e.g. Naab et al. 2009).

In fact, the observations allow the possibility that the central

<sup>6</sup> We exclude cases where the systems are gas-dominated from this discussion, as in these cases the relevant physics leads to qualitatively different behavior in mergers, and will not necessarily make spheroids at all (Robertson et al. 2006; Hopkins et al. 2009b,f).

regions of some massive ellipticals today have evolved with little or no strong perturbation, and corresponding change in densities, since high redshifts, while their envelopes assemble over this same period in time. This is important for the kinds of mergers that influence bulge formation: mergers with the kinds of low-density systems needed to build up an extended, low-density envelope (minor mergers, mergers with relatively gas-poor disks, and mergers with later-forming, less dense ellipticals) will not significantly perturb the (much more dense) central regions of the galaxy. In detail, even equal mass mergers with equal density systems do significantly less to lower than central densities than a simple energetic argument would imply: the central density profile remains relatively unperturbed while energy tends to be preferentially transferred to less bound outer material (see Hopkins et al. 2009d).

Such mergers may also transform an initial central “cuspy” profile into a “cored” profile, via the scouring action of a binary BH-BH merger (if the initial high-redshift systems are “cuspy,” expected if they have just formed in gas-rich mergers, then they must become cored by low-redshift to correspond to observed systems; see e.g. Faber et al. 1997; Graham et al. 2003; Côté et al. 2007; Kormendy et al. 2009). Both minor and major dry mergers are expected to be efficient mechanisms for scouring, even where the secondary is sufficiently low density so as not to perturb the density profile as discussed above (see e.g. Milosavljević et al. 2002). But the cusp-core distinction (in all but the most extreme systems) affects the mass profile only on very small scales (well below the scales observed in all but the nearest systems) and involves only a very small fraction of the galaxy mass ( $\sim M_{\text{BH}}$ , or  $\sim 10^{-3} M_*$ ).

### 6.3 Observational Tests and Future Prospects

Observed high-redshift systems require the growth of extended, low surface density envelopes to match the profiles of massive ellipticals today. It is quite possible that such envelopes are entirely absent at high redshifts. However, Figure 6 highlights the fact that it remains difficult to say precisely how much of a “mass deficit” at large radii must be accreted from  $z = 2$  to  $z = 0$ . In short, the total mass at very low surface densities at high redshifts remains more uncertain than the mass budget at high surface densities. And even where observations detect light at relatively low surface brightness, the relevant  $S/N$  weighting means that the profile fits can be preferentially weighted towards the high-brightness central regions. As a result, there could remain some non-trivial differences in the best-fit  $R_e$  from high-redshift observations, compared to deep low-redshift observations of analogous systems.

At low and intermediate stellar masses, where Sérsic indices tend to be low ( $n_s \lesssim 4$ ), our simple experiments, as well as those in other works calibrated to the specific observation techniques used therein (see e.g. Zirm et al. 2007; Trujillo et al. 2006b, 2007; van der Wel et al. 2008; Cimatti et al. 2008), suggest that there is no strong dependence on the depth of the observations. In other words, when there is no significant envelope, the precise mass profile of the low-density material makes little difference. At the highest masses, however – i.e. local systems where the outer Sérsic indices are very large ( $n_s \gtrsim 6$ ) because of the presence of large stellar envelopes that can extend to  $\gtrsim 100\text{kpc}$  scales – there can be a non-trivial mass at extremely low brightness, whose profile is difficult to recover in detail. If massive-envelope ellipticals such as NGC 4552 were present at  $z > 0.5$ , full recovery of their envelopes (in the sense of recovering high  $S/N$  profile information) would require observations  $\sim 4 - 5$  mag deeper than typical of individual high-redshift objects (Figure 6). Even at low redshifts, only a

small fraction of objects at the highest masses have *directly* measured and converged effective radii (determined purely from the observed light profile); in other cases the effective radius is usually estimated by extrapolation of a best-fit Sérsic profile to low densities and large radii. It is possible, if envelopes are present, but do not follow a perfect Sérsic profile (or if the Sérsic profile shape of the galaxy profile changes from small to large radii), to underestimate the envelope mass, and correspondingly to underestimate the true effective radius by a factor  $\sim 2$ .

This has important consequences even at low redshifts. Some recent studies have claimed that *most* of the apparent size-mass evolution in massive galaxies occurs at very low redshifts, a factor of  $\sim 2 - 3$  change in sizes between  $z = 0.1 - 0.3$ , with the evolution from  $z = 0.4 - 2$  restricted to a smaller factor  $\sim 1.5 - 2$  (Bernardi 2009; Ferreras et al. 2009). Such extreme apparent low-redshift evolution (as opposed to the more plausible high-redshift evolution) may be related to the observed dynamic range and fitting: it is almost impossible to explain such a large change in the true stellar half-mass radius in any model over a narrow low-redshift interval  $z = 0.1 - 0.3$ . Independent constraints have clearly established that in this redshift range, there is almost no evolution in the stellar mass function of massive spheroids, nor is there significant evolution in the (uniformly old) stellar populations, or any significant stellar mass loss or new star formation given the old stellar population ages (Thomas et al. 2005; Nelan et al. 2005; Gallazzi et al. 2006; Masjedi et al. 2006; Borch et al. 2006; Jones et al. 2006). Likewise, there is no change in their kinematics or the fundamental plane relation in clusters or the field (Treu et al. 2005; di Serego Alighieri et al. 2005; van der Wel et al. 2005; van Dokkum & van der Marel 2007). Even the dark matter halos grow by only a tiny fraction over the redshift range of  $z = 0.1$  to  $0.3$  ( $< 0.1$  dex; almost all accreted at large radii). What do change over this redshift range, however, are the spatial resolution and effective surface brightness limits, and as a consequence the radial range of the profile sampled in observations. We find that the observations of rapid changes in the best-fit  $R_e$  at low redshifts can be accounted for by the biases summarized in Figure 6. And indeed, other observations, using somewhat different fitting methodology and sample selection, have found no such significant evolution at low redshifts, while the high-redshift evolution appears more robust (see e.g. McIntosh et al. 2005; Trujillo et al. 2007; Franx et al. 2008).

Clearly, better constraints on just how much low-surface brightness material is present, as a function of redshift, will improve our understanding of elliptical galaxy formation. Whether there has been a great deal of evolution in the amount of low-density material, or relatively little, either result is of considerable interest. If high-redshift systems have essentially no stellar mass at low densities ( $\Sigma \lesssim 10^{9-10} M_\odot \text{kpc}^{-2}$ ), then mergers forming spheroids must initially be very gas-rich, and mergers with lower-mass galaxies or evolved disks at high redshift must be relatively rare. Moreover, this would determine how much material would have to be built up by subsequent mergers, putting requirements on models for tidal destruction and minor mergers as well as later dry major mergers. If some envelopes are present at high redshifts – perhaps not as much as at low redshifts, but still non-negligible in mass – then it would strongly limit the amount of growth, accretion, and dry merging such systems could undergo at lower redshifts. To the extent that envelopes exist that contain significant mass not previously detected, it would increase the stellar masses of these galaxies, perhaps yielding tension with constraints from e.g. the galaxy mass function, and certainly presenting a challenge for

models, which have difficulty explaining very early mass assembly without much subsequent growth.

There are a number of observational means to study these possibilities. Most directly, observations can probe whether such material exists at high redshifts. In addition to profile fitting, which necessarily relies on the assumption that some functional form will represent a good approximation to light at radii where the profile shape cannot be strongly constrained directly, it should be possible to estimate that total light contribution from comparison of deep integrations of the total light/stellar mass in fixed physical annuli. Also, stacking the observed high-redshift systems, allowing for a gain of  $\sim 1 - 1.5$  mag in surface brightness depth, seems to show a continued steep falloff in surface density ( $n_s \lesssim 4$ ), indicating that there is not a large undetected mass in envelopes at high redshift (Zirm et al. 2007; van der Wel et al. 2008). This reinforces the conclusion that the envelopes must be predominantly built up at lower redshifts; unfortunately, it remains difficult to say precisely how much material is at low densities (other than to say that it is not a large fraction of the galaxy mass and cannot change  $R_e$  at the level of evolution seen), or what the exact mass profile of the low-density material is (e.g. whether it corresponds to the inference from extrapolating the fitted Sérsic profiles, cuts off more steeply, or obeys a power law-like distribution analogous to observed intra-cluster/halo light in low-redshift systems).

Observations of major and minor dry merger rates offer complementary constraints on how much material is added to these systems between high redshifts and today. In the local universe, studying the properties of these envelopes can inform models of their formation histories. For example, stellar population gradients and kinematics might reflect a more dramatic transition in properties if the envelopes form by late accretion onto earlier-forming cores. If the envelopes form early, they will be metal poor and have different  $\alpha$ -element abundances compared to late-accreting disk/outer bulge material. Some efforts have been made along these lines (see e.g. Sánchez-Blázquez et al. 2007), and gradients in e.g.  $\alpha$ -element abundances show significant diversity, suggesting that in some systems, envelopes formed quickly (perhaps in e.g. later-forming ellipticals, where a large envelope can be formed from relatively gas-poor disks), while in others, envelopes are contributed by systems with more extended star formation (e.g. late mergers with lower-mass or later-forming systems, as expected for systems described here). However, samples remain small, and the differences are subtle; larger samples are needed to correlate the behavior of these properties with other aspects of galaxies (e.g. galaxy mass, kinematics, cusp/core status, environment) that might provide an indication of whether or not they are descendants of similar high-redshift systems. Moreover, typical observations of these quantities extend only to relatively small radii ( $\sim R_e$ ); it remains difficult to probe stellar populations in the low-density outer regions that constitute spheroid envelopes. Together, however, these observations offer promising avenues towards constraining these observationally challenging, low-surface brightness components.

Corroborating evidence for the picture presented here has recently been presented in Cenarro & Trujillo (2009). The authors measure the average velocity dispersions of compact spheroids at  $z = 0 - 2$ , and show that it evolves weakly relative to e.g. the naive expectation of models with uniform contraction/expansion (that  $\sigma^2 \propto M_*/R_e$ ). Despite factor  $\sim 6$  evolution in effective radii of massive galaxies over this interval, the median  $\sigma$  at fixed mass evolves by a factor  $\approx 1.3$ . Moreover, the high-redshift  $\sigma$  values are in fact consistent with the high end of the observed low-redshift scatter at this mass, or with the median  $\sigma$  of slightly more massive

(factor  $\sim 2$ ) low-redshift ellipticals. This is precisely the behavior expected if the central, high-density regions (which determine the central potential depth and correspondingly  $\sigma$ ) assemble preferentially early, and evolve relatively unperturbed to low redshift (for examples in simulations, see Hopkins et al. 2009c). Low-density material accreted later is clearly important for the effective radii, and changes e.g. the dark matter fraction within  $R_e$  as well as the profile shape, but has very little effect on the velocity dispersion. The observations represent a strong constraint on the physical densities at fixed radius: if the central densities at high redshift were in fact substantially higher than those at low redshift, by even a factor of a few, it would significantly over-predict the observed evolution in velocity dispersions.

Throughout this paper, we have neglected several additional physical effects that might affect estimates of the stellar surface mass densities and effective radii of high-redshift ellipticals. For example, at low redshifts, stellar mass-to-light ratios are independent of radius to within  $\sim 20\%$  in optical bands in massive ellipticals, which tend to be uniformly old and have weak color gradients (see e.g. Faber et al. 1989; Bender et al. 1993). However, given the observed stellar population gradients run backwards in time, or considering local recent merger remnants and/or simulations, the expectation is that this could be quite different at the high redshifts when the ellipticals formed (Schweizer 1996; Rothberg & Joseph 2004; Yamauchi & Goto 2005). The young, post-starburst population (ages  $\lesssim 1 - 2$  Gyr) in the core has higher optical  $L/M_*$ , which can lead to a rest-frame  $B$ -band best-fit  $R_e$  that is a factor  $\sim 1.5 - 2$  smaller than the stellar-mass  $R_e$  (or the  $B$ -band  $R_e$  observed when the system has aged and this effect vanishes). Some reassurance, however, comes from the fact that the size-mass relation does not seem to depend strongly on the precise stellar population age/colors (specifically within the “quenched” or “star-forming” populations; see Pérez-González et al. 2008a; Toft et al. 2007) and the fact that the observed sizes of the galaxies of interest here are similar in rest-frame near-UV and optical (Trujillo et al. 2007). There may also be some bias in estimated stellar masses of systems at similar ages, owing to the uncertain contribution of AGB stars (Maraston 2005; Maraston et al. 2006). This is estimated to be a possible factor  $\sim 1.2 - 1.4$  over-estimate of the high-redshift masses where high-quality optical photometry is available (Wuyts et al. 2007, 2009). We have conservatively ignored these effects, but if present they will strengthen most of our conclusions. To test for these effects, it is important to obtain deeper spectra and photometry, to test for the presence of blue cores and constrain the contribution of stellar populations of different ages (and stellar population gradients) in systems at intermediate and high redshifts.

## ACKNOWLEDGMENTS

We thank Todd Thompson, Ignacio Trujillo, Chien Peng, Pieter van Dokkum, and Marijn Franx for helpful discussions. We also thank the anonymous referee for comments and suggestions regarding the treatment of observational effects. Support for PFH was provided by the Miller Institute for Basic Research in Science, University of California Berkeley. EQ is supported in part by NASA grant NNG06GI68G and the David and Lucile Packard Foundation.

## REFERENCES

Abraham, R. G., et al. 2007, *ApJ*, 669, 184

- Allen, P. D., Driver, S. P., Graham, A. W., Cameron, E., Liske, J., & de Propris, R. 2006, *MNRAS*, 371, 2
- Balcells, M., Graham, A. W., & Peletier, R. F. 2007a, *ApJ*, 665, 1084
- . 2007b, *ApJ*, 665, 1104
- Barden, M., et al. 2005, *ApJ*, 635, 959
- Barnes, J. E., & Hernquist, L. 1996, *ApJ*, 471, 115
- Bell, E. F., McIntosh, D. H., Katz, N., & Weinberg, M. D. 2003, *ApJS*, 149, 289
- Bell, E. F., et al. 2006, *ApJ*, 640, 241
- Bender, R., Burstein, D., & Faber, S. M. 1993, *ApJ*, 411, 153
- Bernardi, M. 2009, *MNRAS*, 395, 1491
- Bernardi, M., Hyde, J. B., Sheth, R. K., Miller, C. J., & Nichol, R. C. 2007, *AJ*, 133, 1741
- Bezanson, R., van Dokkum, P. G., Tal, T., Marchesini, D., Kriek, M., Franx, M., & Coppi, P. 2009, *ApJ*, 697, 1290
- Borch, A., et al. 2006, *A&A*, 453, 869
- Bower, R. G., Benson, A. J., Malbon, R., Helly, J. C., Frenk, C. S., Baugh, C. M., Cole, S., & Lacey, C. G. 2006, *MNRAS*, 370, 645
- Boylan-Kolchin, M., Ma, C.-P., & Quataert, E. 2006, *MNRAS*, 369, 1081
- Brown, M. J. I., Zheng, Z., White, M., Dey, A., Jannuzi, B. T., Benson, A. J., Brand, K., Brodwin, M., & Croton, D. J. 2008, *ApJ*, 682, 937
- Buitrago, F., Trujillo, I., Conselice, C. J., Bouwens, R. J., Dickinson, M., & Yan, H. 2008, *ApJL*, 687, L61
- Burkert, A., Naab, T., Johansson, P. H., & Jesseit, R. 2008, *ApJ*, 685, 897
- Cenarro, A. J., & Trujillo, I. 2009, *ApJL*, 696, L43
- Chabrier, G. 2003, *PASP*, 115, 763
- Cimatti, A., et al. 2008, *A&A*, 482, 21
- Conroy, C., & Wechsler, R. H. 2009, *ApJ*, 696, 620
- Côté, P., et al. 2006, *ApJS*, 165, 57
- . 2007, *ApJ*, 671, 1456
- Cox, T. J., Dutta, S. N., Di Matteo, T., Hernquist, L., Hopkins, P. F., Robertson, B., & Springel, V. 2006, *ApJ*, 650, 791
- Daddi, E., et al. 2005, *ApJ*, 626, 680
- Damjanov, I., et al. 2009, *ApJ*, 695, 101
- di Serego Alighieri, S., et al. 2005, *A&A*, 442, 125
- Faber, S. M., Tremaine, S., Ajhar, E. A., Byun, Y.-I., Dressler, A., Gebhardt, K., Grillmair, C., Kormendy, J., Lauer, T. R., & Richstone, D. 1997, *AJ*, 114, 1771
- Faber, S. M., Wegner, G., Burstein, D., Davies, R. L., Dressler, A., Lynden-Bell, D., & Terlevich, R. J. 1989, *ApJS*, 69, 763
- Ferguson, H. C., et al. 2004, *ApJL*, 600, L107
- Ferrarese, L., et al. 2006, *ApJS*, 164, 334
- Ferreras, I., Lisker, T., Pasquali, A., Khochfar, S., & Kaviraj, S. 2009, *MNRAS*, 397, 637
- Fontana, A., et al. 2006, *A&A*, 459, 745
- Franx, M., van Dokkum, P. G., Schreiber, N. M. F., Wuyts, S., Labbé, I., & Toft, S. 2008, *ApJ*, 688, 770
- Gallagher, III, J. S., & Ostriker, J. P. 1972, *AJ*, 77, 288
- Gallazzi, A., Charlot, S., Brinchmann, J., & White, S. D. M. 2006, *MNRAS*, 370, 1106
- Graham, A. W., Erwin, P., Trujillo, I., & Asensio Ramos, A. 2003, *AJ*, 125, 2951
- Graves, G. J., Faber, S. M., & Schiavon, R. P. 2009, *ApJ*, 698, 1590
- Grazian, A., et al. 2007, *A&A*, 465, 393
- Hausman, M. A., & Ostriker, J. P. 1978, *ApJ*, 224, 320
- Hernquist, L., Spergel, D. N., & Heyl, J. S. 1993, *ApJ*, 416, 415
- Hibbard, J. E., & Yun, M. S. 1999, *ApJL*, 522, L93
- Hopkins, P. F., Cox, T. J., Dutta, S. N., Hernquist, L., Kormendy, J., & Lauer, T. R. 2009a, *ApJS*, 181, 135
- Hopkins, P. F., Cox, T. J., & Hernquist, L. 2008a, *ApJ*, 689, 17
- Hopkins, P. F., Cox, T. J., Younger, J. D., & Hernquist, L. 2009b, *ApJ*, 691, 1168
- Hopkins, P. F., Hernquist, L., Cox, T. J., Dutta, S. N., & Rothberg, B. 2008b, *ApJ*, 679, 156
- Hopkins, P. F., Hernquist, L., Cox, T. J., Kereš, D., & Wuyts, S. 2009c, *ApJ*, 691, 1424
- Hopkins, P. F., Hernquist, L., Cox, T. J., Robertson, B., & Krause, E. 2007a, *ApJ*, 669, 45
- . 2007b, *ApJ*, 669, 67
- Hopkins, P. F., Lauer, T. R., Cox, T. J., Hernquist, L., & Kormendy, J. 2009d, *ApJS*, 181, 486
- Hopkins, P. F., Lidz, A., Hernquist, L., Coil, A. L., Myers, A. D., Cox, T. J., & Spergel, D. N. 2007c, *ApJ*, 662, 110
- Hopkins, P. F., Murray, N., & Thompson, T. A. 2009e, *MNRAS*, 398, 303
- Hopkins, P. F., Somerville, R. S., Cox, T. J., Hernquist, L., Jogee, S., Kereš, D., Ma, C.-P., Robertson, B., & Stewart, K. 2009f, *MNRAS*, 397, 802
- Jesseit, R., Naab, T., Peletier, R. F., & Burkert, A. 2007, *MNRAS*, 376, 997
- Jones, D. H., Peterson, B. A., Colless, M., & Saunders, W. 2006, *MNRAS*, 369, 25
- Kennicutt, Jr., R. C. 1998, *ApJ*, 498, 541
- Khochfar, S., & Silk, J. 2006, *ApJL*, 648, L21
- Komatsu, E., et al. 2009, *ApJS*, 180, 330
- Kormendy, J. 1999, in *Astronomical Society of the Pacific Conference Series*, Vol. 182, *Galaxy Dynamics - A Rutgers Symposium*, ed. D. R. Merritt, M. Valluri, & J. A. Sellwood, 124–+
- Kormendy, J., Fisher, D. B., Cornell, M. E., & Bender, R. 2009, *ApJS*, 182, 216
- Kriek, M., van der Wel, A., van Dokkum, P. G., Franx, M., & Illingworth, G. D. 2008a, *ApJ*, 682, 896
- Kriek, M., et al. 2006, *ApJL*, 649, L71
- . 2008b, *ApJ*, 677, 219
- Labbé, I., et al. 2005, *ApJL*, 624, L81
- Lauer, T. R., et al. 2007, *ApJ*, 664, 226
- Lin, L., et al. 2008, *ApJ*, 681, 232
- Maraston, C. 2005, *MNRAS*, 362, 799
- Maraston, C., Daddi, E., Renzini, A., Cimatti, A., Dickinson, M., Papovich, C., Pasquali, A., & Pirzkal, N. 2006, *ApJ*, 652, 85
- Marchesini, D., van Dokkum, P. G., Forster Schreiber, N. M., Franx, M., Labbé, I., & Wuyts, S. 2008, *ApJ*, in press, arXiv:0811.1773 [astro-ph]
- Masjedi, M., et al. 2006, *ApJ*, 644, 54
- McIntosh, D. H., et al. 2005, *ApJ*, 632, 191
- Mihos, J. C., & Hernquist, L. 1994, *ApJL*, 437, L47
- Milosavljević, M., Merritt, D., Rest, A., & van den Bosch, F. C. 2002, *MNRAS*, 331, L51
- Naab, T., Jesseit, R., & Burkert, A. 2006, *MNRAS*, 372, 839
- Naab, T., Johansson, P. H., & Ostriker, J. P. 2009, *ApJ*, in press, arXiv:0903.1636
- Naab, T., Johansson, P. H., Ostriker, J. P., & Efstathiou, G. 2007, *ApJ*, 658, 710
- Nelan, J. E., et al. 2005, *ApJ*, 632, 137
- Oñorbe, J., Domínguez-Tenreiro, R., Sáiz, A., Artal, H., & Serna, A. 2006, *MNRAS*, 373, 503
- Ostriker, J. P., & Tremaine, S. D. 1975, *ApJL*, 202, L113
- Pérez-González, P. G., Trujillo, I., Barro, G., Gallego, J., Zamorano, J., & Conselice, C. J. 2008a, *ApJ*, 687, 50

- Pérez-González, P. G., et al. 2008b, *ApJ*, 675, 234
- Quadri, R., et al. 2007, *ApJ*, 654, 138
- Ravindranath, S., et al. 2004, *ApJL*, 604, L9
- Robertson, B., Bullock, J. S., Cox, T. J., Di Matteo, T., Hernquist, L., Springel, V., & Yoshida, N. 2006, *ApJ*, 645, 986
- Rothberg, B., & Joseph, R. D. 2004, *AJ*, 128, 2098
- Sánchez-Blázquez, P., Forbes, D. A., Strader, J., Brodie, J., & Proctor, R. 2007, *MNRAS*, 377, 759
- Schweizer, F. 1996, *AJ*, 111, 109
- Shapiro, K. L., et al. 2008, *ApJ*, 682, 231
- Shen, S., Mo, H. J., White, S. D. M., Blanton, M. R., Kauffmann, G., Voges, W., Brinkmann, J., & Csabai, I. 2003, *MNRAS*, 343, 978
- Somerville, R. S., et al. 2008, *ApJ*, 672, 776
- Tacconi, L. J., Neri, R., Chapman, S. C., Genzel, R., Smail, I., Ivison, R. J., Bertoldi, F., Blain, A., Cox, P., Greve, T., & Omont, A. 2006, *ApJ*, 640, 228
- Tacconi, L. J., et al. 2008, *ApJ*, 680, 246
- Thomas, D., Maraston, C., Bender, R., & Mendes de Oliveira, C. 2005, *ApJ*, 621, 673
- Thompson, T. A., Quataert, E., & Murray, N. 2005, *ApJ*, 630, 167
- Toft, S., et al. 2007, *ApJ*, 671, 285
- Trager, S. C., Faber, S. M., Worthey, G., & González, J. J. 2000, *AJ*, 119, 1645
- Treu, T., et al. 2005, *ApJ*, 633, 174
- Trujillo, I., Asensio Ramos, A., Rubiño-Martín, J. A., Graham, A. W., Aguerri, J. A. L., Cepa, J., & Gutiérrez, C. M. 2002, *MNRAS*, 333, 510
- Trujillo, I., Cenarro, A. J., de Lorenzo-Cáceres, A., Vazdekis, A., de la Rosa, I. G., & Cava, A. 2009, *ApJL*, 692, L118
- Trujillo, I., Conselice, C. J., Bundy, K., Cooper, M. C., Eisenhardt, P., & Ellis, R. S. 2007, *MNRAS*, 382, 109
- Trujillo, I., et al. 2004, *ApJ*, 604, 521
- . 2006a, *MNRAS*, 373, L36
- . 2006b, *ApJ*, 650, 18
- van der Wel, A., Bell, E. F., van den Bosch, F. C., Gallazzi, A., & Rix, H.-W. 2009, *ApJ*, 698, 1232
- van der Wel, A., Franx, M., van Dokkum, P. G., Rix, H.-W., Illingworth, G. D., & Rosati, P. 2005, *ApJ*, 631, 145
- van der Wel, A., Holden, B. P., Zirm, A. W., Franx, M., Rettura, A., Illingworth, G. D., & Ford, H. C. 2008, *ApJ*, 688, 48
- van Dokkum, P., et al. 2008, *ApJL*, 677, L5
- van Dokkum, P. G. 2005, *AJ*, 130, 2647
- van Dokkum, P. G., & van der Marel, R. P. 2007, *ApJ*, 655, 30
- van Dokkum, P. G., et al. 2006, *ApJL*, 638, L59
- Weil, M. L., & Hernquist, L. 1994, *ApJL*, 431, L79
- . 1996, *ApJ*, 460, 101
- Wuyts, S., Franx, M., Cox, T. J., Hernquist, L., Hopkins, P. F., Robertson, B. E., & van Dokkum, P. G. 2009, *ApJ*, 696, 348
- Wuyts, S., et al. 2007, *ApJ*, 655, 51
- Yamauchi, C., & Goto, T. 2005, *MNRAS*, 359, 1557
- Younger, J. D., et al. 2007, *ApJ*, 671, 1531
- . 2008, *ApJ*, 688, 59
- Zheng, Z., Coil, A. L., & Zehavi, I. 2007, *ApJ*, 667, 760
- Zirm, A. W., et al. 2007, *ApJ*, 656, 66